


Transparent boundary condition for simulating rogue wave solutions in the nonlinear Schrödinger equation

Chenxi Zheng and Shaoqiang Tang ^{*}

Key Laboratory of High Energy Density Physics Simulations, Ministry of Education, State Key Laboratory of Turbulence and Complex Systems, College of Engineering, Peking University, Beijing 100871, China

 (Received 26 May 2022; accepted 6 October 2022; published 7 November 2022)

This paper addresses the construction of numerical boundary conditions for simulating rogue wave solutions in the nonlinear Schrödinger equation. While three kinds of commonly used boundary conditions require a big enough computational domain to reproduce solutions faithfully in the central domain, we propose transparent boundary conditions for the Peregrine soliton and Kuznetsov-Ma breather solutions, respectively. For both solutions, these boundary conditions require a smaller computational domain than other boundary conditions to attain the best accuracy of the Crank-Nicolson scheme and selected mesh size, which will be referred to as the “acceptable accuracy” below. In particular, the computational domain with these boundary conditions is only 1/16 as small as others in the simulations of the Peregrine soliton solution. As a result, they reduce both the memory requirement and the computing time for the Peregrine soliton solution.

DOI: [10.1103/PhysRevE.106.055302](https://doi.org/10.1103/PhysRevE.106.055302)

I. INTRODUCTION

A rogue wave is also known as a freak wave, a monster wave, a killer wave, and a giant wave. It was originally identified in oceanography as a wave whose height is bigger than twice the significant wave height. Then it was extended to nonlinear fiber optics, plasmas, Bose-Einstein condensates, etc. [1–4].

The most commonly used model for rogue waves is the focusing nonlinear Schrödinger (NLS) equation

$$iu_t + \frac{1}{2}u_{xx} + |u|^2u = 0, \quad (1)$$

where i is the imaginary unit, and the modulus of the complex variable $u(x, t)$ describes the modulation of a carrier wave in the water waves or the density in quantum mechanics. The most notable solution with the form

$$u_{\text{PS}}(x, t) = \left[1 - \frac{4(1 + 2it)}{1 + 4x^2 + 4t^2} \right] e^{it} \quad (2)$$

is called the Peregrine soliton (PS) solution [5]. It decays in both space and time, which coincides with the feature of rogue waves that appear out of nowhere and disappear without a trace [6]. Another crucial solution is the so-called Kuznetsov-Ma breather (KB) solution [7,8],

$$u_{\text{KB}}(x, t; T) = \left[1 + \frac{2(1 - 2a) \cos(\Omega t) - i\Omega \sin(\Omega t)}{\sqrt{2a} \cosh(bx) - \cos(\Omega t)} \right] e^{it}, \quad (3)$$

where $\Omega = 2\pi/T$, $a = (1 + \sqrt{\Omega^2 + 1})/4$, and $b = 2\sqrt{2a - 1}$. It is spatially local and temporally periodic with the period T . The KB solution reduces to the PS solution in the limit in which the period T tends to infinity. The PS and KB solutions both decay to a nonzero background e^{it} as x

tends to infinity. They are natural candidates of rogue waves, and they are known as rogue wave solutions.

To study the rogue wave solutions numerically, the original problem is usually truncated into a bounded computational domain. There are extensive studies on boundary conditions for simulating solutions decaying to zero at infinity. The absorbing boundary condition is the one in which some energy functional is absorbed at the boundary. For example, the perfectly matched layer method adds nonphysical absorbing field components adjacent to the computational boundary [9,10]. For another example, the far-field boundary conditions are obtained by the Laplace transform and a high frequency expansion of solutions, which identify and absorb the outgoing waves [11–13]. Another kind of boundary condition is referred as a transparent boundary condition if the approximate solution actually coincides in the interior domain with the exact solution for the whole space problem. These boundary conditions are usually obtained by solving the exterior problems. See [14–17] and references therein for more details about transparent boundary conditions. Matching boundary conditions and almost exact boundary conditions are some other accurate and efficient numerical boundary conditions [18–20].

However, significant difficulties and numerical instabilities arise due to the nonzero background. Dirichlet, Neumann, and periodic boundary conditions are commonly used, yet they require a large computational domain to prevent the artifact of numerical boundaries. To our knowledge, there is not much work on designing transparent boundary conditions with nonzero far-field conditions for the NLS equation. Birem and Klein proposed a multidomain spectral method based on a Möbius transformation that maps the infinite line to a bounded domain [21]. Islas and Schober developed a Chebyshev pseudospectral method to simulate in the infinite spatial domain [22]. Wang *et al.* derived a boundary treatment of arbitrary order based on the far-field asymptotic expansion [23].

^{*}Corresponding author: maotang@pku.edu.cn

The main focus of this work is to develop a boundary treatment by discretizing the time-independent equations that rogue wave solutions satisfy. This treatment is referred to as the time-independent transparent boundary condition (TITBC) below. To attain the best accuracy with the Crank-Nicolson scheme and fixed mesh size, simulations with the TITBC can be performed in a much smaller domain than three commonly used boundary conditions, especially only 1/16 for the PS solution simulation. The rest of this paper is organized as follows. In Sec. II, we introduce the numerical scheme and the TITBC for both KB and PS solutions. In Sec. III, we provide numerical evidence showing that simulations with the TITBC can be performed in a rather small domain to attain an “acceptable accuracy,” with the meaning to be precisely stated. Finally, we draw conclusions and put some further proposals in Sec. IV.

II. NUMERICAL METHODS

We truncate the computational domain from the whole spatial domain to a finite one $[x_l, x_r]$ with width $W = x_r - x_l$. With a time step size k and mesh size $h = (x_r - x_l)/M$, we denote the grid points and time steps as

$$x_m = x_l + mh, \quad t_n = t_0 + nk. \tag{4}$$

The numerical approximation of $u(x_m, t_n)$ is u_m^n . For ease of presentation, we introduce finite-difference operators

$$D_h^0 u_m^n = \frac{u_{m+1}^n - u_{m-1}^n}{2h}, \tag{5}$$

$$D_h^2 u_m^n = \frac{u_{m+1}^n - 2u_m^n + u_{m-1}^n}{h^2}, \tag{6}$$

$$D_h^4 u_m^n = \frac{u_{m+2}^n - 4u_{m+1}^n + 6u_m^n - 4u_{m-1}^n + u_{m-2}^n}{h^4}. \tag{7}$$

We use the Crank-Nicolson scheme for the NLS equation proposed by Delfour *et al.* [24]:

$$i \frac{u_m^{n+1} - u_m^n}{k} + \frac{1}{2} D_h^2 \left(\frac{u_m^{n+1} + u_m^n}{2} \right) + \left(\frac{|u_m^{n+1}|^2 + |u_m^n|^2}{2} \right) \left(\frac{u_m^{n+1} + u_m^n}{2} \right) = 0, \tag{8}$$

where $m = 0, \dots, M$. This scheme is unconditionally stable and has the mass and energy conservation properties [24]. The Crank-Nicolson scheme is an implicit scheme, so a nonlinear algebraic system should be solved at each time step. We solve the system by the fixed point iteration method, and we take the value in the preceding step as an initial guess for the subsequent step.

We remark that there are two popular forms of Crank-Nicolson schemes for the NLS equation. One is the scheme (8), which was used in [15,16]. Another one handles the nonlinear term as $|u_m^{n+1}|^2 u_m^{n+1} + |u_m^n|^2 u_m^n$ [25]. Our simulations show that the pointwise relative differences between these two forms are under 0.5% for tests in this work. The form of the Crank-Nicolson scheme has little effect on numerical results.

The system (8) needs two more equations of points out of our computational domain, namely u_{-1}^{n+1} and u_{M+1}^{n+1} , to be

closed. Three kinds of numerical boundary conditions introduced below are widely used.

(i) Dirichlet boundary condition. For both PS and KB solutions, u tends to e^{it} as x approaches infinity. This provides a simple far-field condition:

$$u_{-1}^{n+1} = u_{M+1}^{n+1} = e^{it_{n+1}}. \tag{9}$$

(ii) Neumann boundary condition. For both PS and KB solutions, the derivative u_x tends to zero as x approaches infinity. By the central difference method, it suggests the boundary conditions

$$\frac{u_1^{n+1} - u_{-1}^{n+1}}{2h} = \frac{u_{M+1}^{n+1} - u_{M-1}^{n+1}}{2h} = 0. \tag{10}$$

(iii) Periodic boundary condition. The spectral method is widely used to simulate the NLS equation, which naturally assumes that the boundary is periodic. We implement the periodic boundary condition by setting the points

$$u_{-1}^{n+1} = u_{M-1}^{n+1}, \quad u_{M+1}^{n+1} = u_1^{n+1} \tag{11}$$

in the finite-difference method. In our simulations, we notice that the numerical solutions are symmetric in space because of the symmetry of the initial data and the computational domain. This suggests that $u_{M-1}^{n+1} = u_1^{n+1}$. As a result, our simulations with periodic boundary conditions also satisfy the Neumann boundary conditions (10). There is no difference between the numerical solutions with Neumann and periodic boundary conditions by the same setting. So we only show the Neumann one below.

As we shall see in a while, these boundary conditions would require a very large computational domain to attain an “acceptable accuracy,” whose meaning will be explained in Sec. III A. We design the TITBC according to the properties of rogue wave solutions.

(i) For $u = u_{PS}$, u satisfies

$$u_{xxxx} + 6u_x^2 \bar{u} + 2(4|u|^2 - 3)u_{xx} + 2u^2 \bar{u}_{xx} + 4|u_x|^2 u + 6(|u|^2 - 1)^2 u = 0. \tag{12}$$

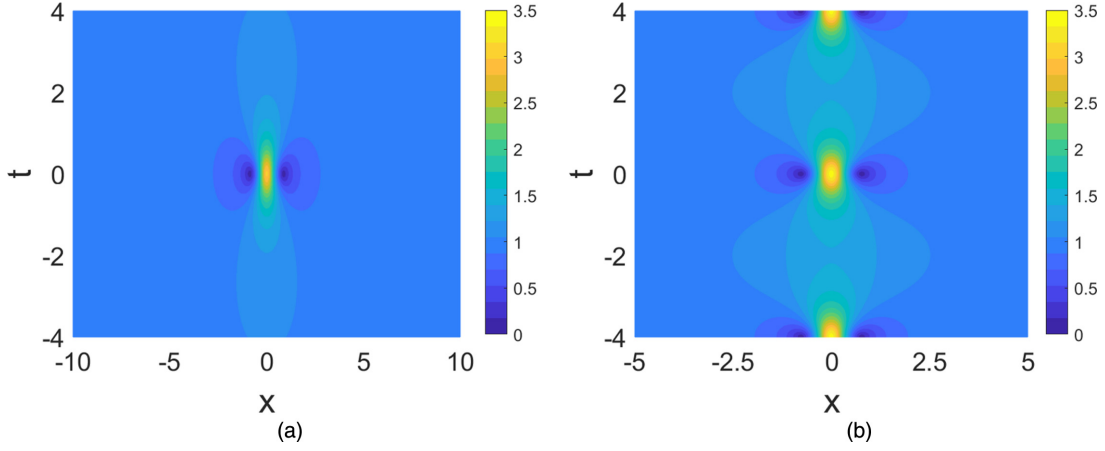
(ii) For $u = u_{KB}$, u satisfies

$$u_{xxxx} + 6u_x^2 \bar{u} + 2(4|u|^2 - 3)u_{xx} + 2u^2 \bar{u}_{xx} + 4|u_x|^2 u + 6(|u|^2 - 1)^2 u - b^2 [u_{xx} + 2u(|u|^2 - 1)] = 0, \tag{13}$$

where the parameter b is the same as that shown in (3).

See Theorem 2.1 in [26] for details. As far as we know, that was the first time that a rogue wave solution was proven to satisfy a time-independent equation. Note that (12) is directly obtained by taking the limit of (13) in which b tends to zero. This agrees with the fact that the PS solution is a limiting behavior of the KB solution.

We remark that neither (12) nor (13) serves as an appropriate boundary condition to form a general initial-boundary-value problem of (1), as their spatial differentiation orders are higher than 1. As we know, this problem needs a boundary condition with maximal order 1 in the space to be well-posed [27]. Nevertheless, (12) and (13) turn out to be capable of capturing correctly the specific rogue wave solution of interest in this work.


 FIG. 1. The rogue wave solutions $|u|$: (a) PS; (b) KB with $T = 4$.

We propose the following discretization for the left-hand side of (12):

$$\begin{aligned} \Delta_{PS}(u_m^{n+1}) = & D_h^4 u_m^{n+1} + 6\bar{u}_m^{n+1} (D_h^0 u_m^{n+1})^2 \\ & + 2(4|u_m^{n+1}|^2 - 3)D_h^2 u_m^{n+1} \\ & + 2(u_m^{n+1})^2 D_h^2 \bar{u}_m^{n+1} + 4u_m^{n+1} |D_h^0 u_m^{n+1}|^2 \\ & + 6(|u_m^{n+1}|^2 - 1)^2 u_m^{n+1}. \end{aligned} \quad (14)$$

The TITBC for the PS solution then reads

$$\Delta_{PS}(u_1^{n+1}) = \Delta_{PS}(u_{M-1}^{n+1}) = 0. \quad (15)$$

These are additional equations of u_{-1}^{n+1} and u_{M+1}^{n+1} , respectively. Solving the nonlinear systems (8) and (15) together gives the result at each time step.

Similarly, we discretize the left-hand side of (13) by

$$\Delta_{KB}(u_m^{n+1}) = \Delta_{PS}(u_m^{n+1}) - b^2 [D_h^2 u_m^{n+1} + 2u_m^{n+1} (|u_m^{n+1}|^2 - 1)]. \quad (16)$$

The TITBC for the KB solution reads

$$\Delta_{KB}(u_1^{n+1}) = \Delta_{KB}(u_{M-1}^{n+1}) = 0. \quad (17)$$

III. NUMERICAL RESULT

In this section, the validity of the TITBC for rogue wave solutions is verified numerically. Simulations are performed with the time step size $k = 10^{-4}$ and mesh size $h = 5 \times 10^{-3}$. Recall that the spatial computational domain is $[-W/2, W/2]$ with the width W .

A. Numerical simulations of the KB solution

We simulate with a fixed time period $T = 4$ in this subsection. The corresponding b is $(\sqrt{\pi^2 + 4} - 2)^{1/2}$. We simulate the KB solution for $t \in [-4, 4]$, namely for two periods. Figure 2 shows the numerical solution in $(x, t) \in [-5, 5] \times [-4, 4]$ with different numerical boundary conditions. Figure 2(c), the simulation with the TITBC, looks the same as the exact KB solution in Fig. 1(b). In Fig. 2, three boundary conditions all faithfully reproduce the second peak at $t = 0$. However, the third peak, which is supposed to appear at $t = 4$, is correctly reproduced only in the simulation with the TITBC. The third peak delays in the Dirichlet case, and it advances in the Neumann one. In Fig. 2(d), spurious oscillations are observed in these two simulations at the end.

The main phenomenon of rogue waves is observed in the central domain. We calculate the relative error $e(t_n)$ in the spatial interval $[-2.5, 2.5]$ by the trapezoidal rule to explore the evolution of numerical errors quantitatively. It reads

$$e(t_n) = \frac{\sqrt{\frac{|\Delta u(-2.5, t_n)|^2}{2} + \sum_{j=1}^{5/h-1} |\Delta u(-2.5 + jh, t_n)|^2 + \frac{|\Delta u(2.5, t_n)|^2}{2}}}{\sqrt{\frac{|u_{\text{exact}}(-2.5, t_n)|^2}{2} + \sum_{j=1}^{5/h-1} |u_{\text{exact}}(-2.5 + jh, t_n)|^2 + \frac{|u_{\text{exact}}(2.5, t_n)|^2}{2}}}, \quad (18)$$

where $\Delta u(x_m, t_n) = u_m^n - u_{\text{exact}}(x_m, t_n)$ is the difference between the numerical and exact solution u_{exact} . The exact solution u_{exact} is $u_{\text{KB}}(x, t; 4)$ in this subsection, and it will be referred to as $u_{\text{PS}}(x, t)$ in the next subsection. The relative error is the numerical approximation of the relative L^2 error $(\int_{[-2.5, 2.5]} |\Delta u|^2 dx)^{1/2} / (\int_{[-2.5, 2.5]} |u_{\text{exact}}|^2 dx)^{1/2}$, and

quantitatively measures numerical error in the watch window $[-2.5, 2.5]$.

Figures 3(a) and 3(b) show the effect of the Dirichlet and Neumann boundary conditions, respectively. When the width $W = 10$, the errors of these two boundary conditions stem from roundoff errors and grow rapidly to bigger than

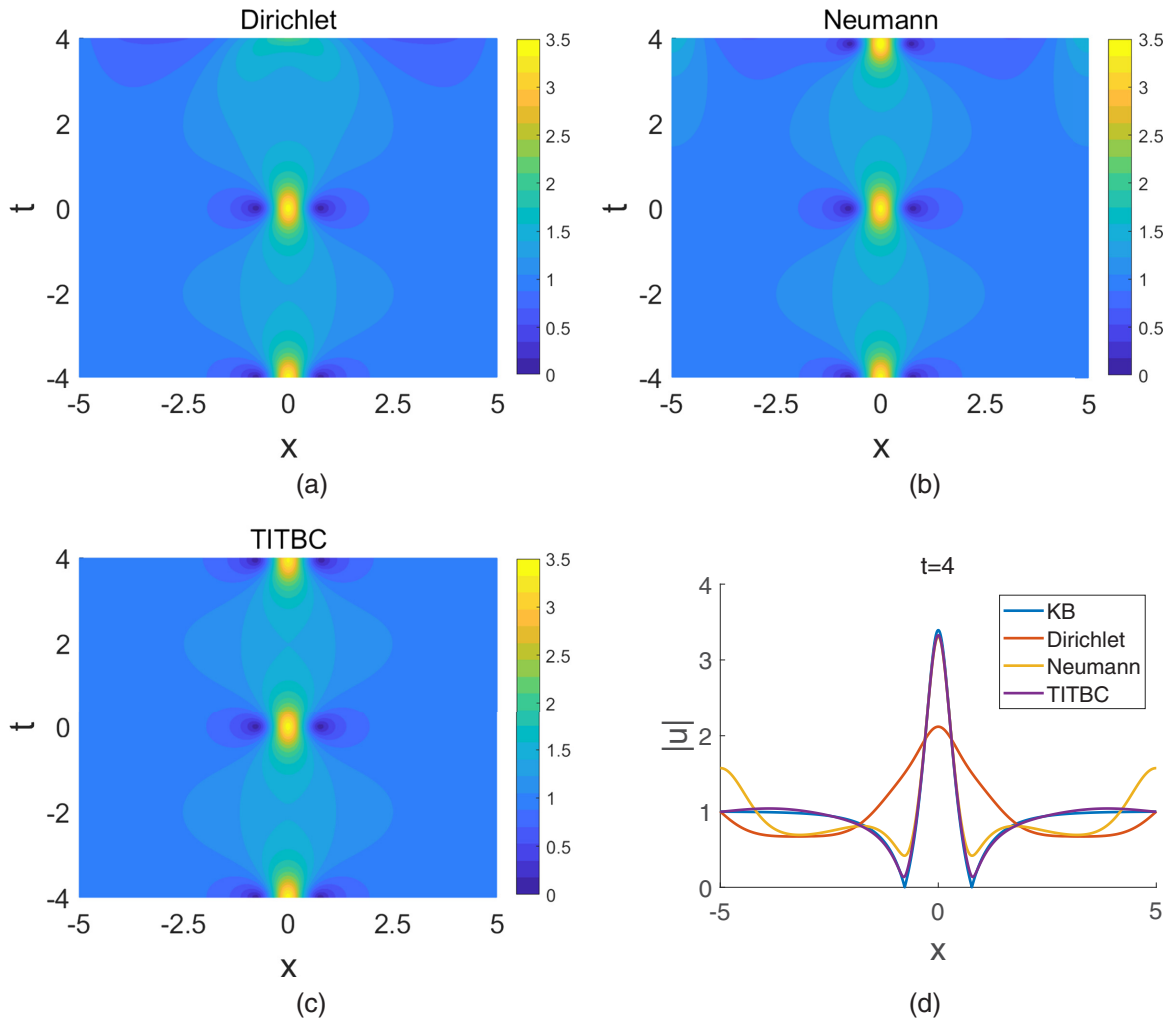


FIG. 2. The numerical result $|u|$ of the KB solution with different numerical boundary conditions: (a) Dirichlet; (b) Neumann; (c) TITBC; (d) $t = 4$.

1×10^{-4} . Then they grow up slowly and reach an observable level $O(1)$ at the end, namely at $t \sim 4$. These correspond to the fact that the second peak is correctly resolved and the third one is disturbed, as shown in Fig. 2. Figure 3(a) shows that the error with $W = 5$ becomes observable at $t \sim -1$. It corresponds to the fact that the second peak is also disturbed in Fig. 3(d). When the width is bigger than 10, the errors become smaller. Moreover, these errors evolve in the same way regardless of width, $W = 20, 40, 80$. Figure 3(c) shows that the errors with the TITBC are almost unaffected by the width. These errors grow in the same way as those by Dirichlet and Neumann with the width $W \geq 20$. This special growth curve of error may be regarded as the lower bound of errors for double precision computations at the selected mesh size. As we verified in [28], the truncation error would grow under the mechanism of modulational instability regardless of the discretization method. To our knowledge, this kind of error in the simulations has been unavoidable up to now. It leads to the lower bound of the errors. When the growth of the relative error approaches this lower bound dictated by the instability, the error in the watch window $[-2.5, 2.5]$ stems from the truncation error in the spatial discretization,

and the effect of boundary conditions is eliminated. We refer to this situation as obtaining an “acceptable accuracy.” Figure 3 indicates that, to reach the “acceptable accuracy” in the simulations of the KB solution, the TITBC can be implemented in a computational domain of 5 in width, which is of one-quarter size compared to the widely used boundary conditions.

To be more specific, the lower bound of errors in Fig. 3 is reached at a big enough width, as the numerical boundary is too far away to affect the central domain. The truncation error in the spatial discretization plays a main role. With such an error evolution, the numerical results in the central domain $[-2.5, 2.5]$ cannot be distinguished. Figure 4 shows the modulus $|\Delta u(x, 4)|$ for the numerical simulation with the TITBC and the width $W = 5$. The main error is around $x \sim 0$, and the error close to $x = \pm 2.5$ is negligible. To explore the effect of the spatial discretization schemes, we simulate with different mesh sizes and show corresponding lower bounds of errors in Fig. 5. The error curves are parallel before the errors reach an observable level $O(1)$. Taking $t = 0$ as the point of comparison, we find that the errors are positively associated with the mesh sizes at the order of 1.96. This agrees well with

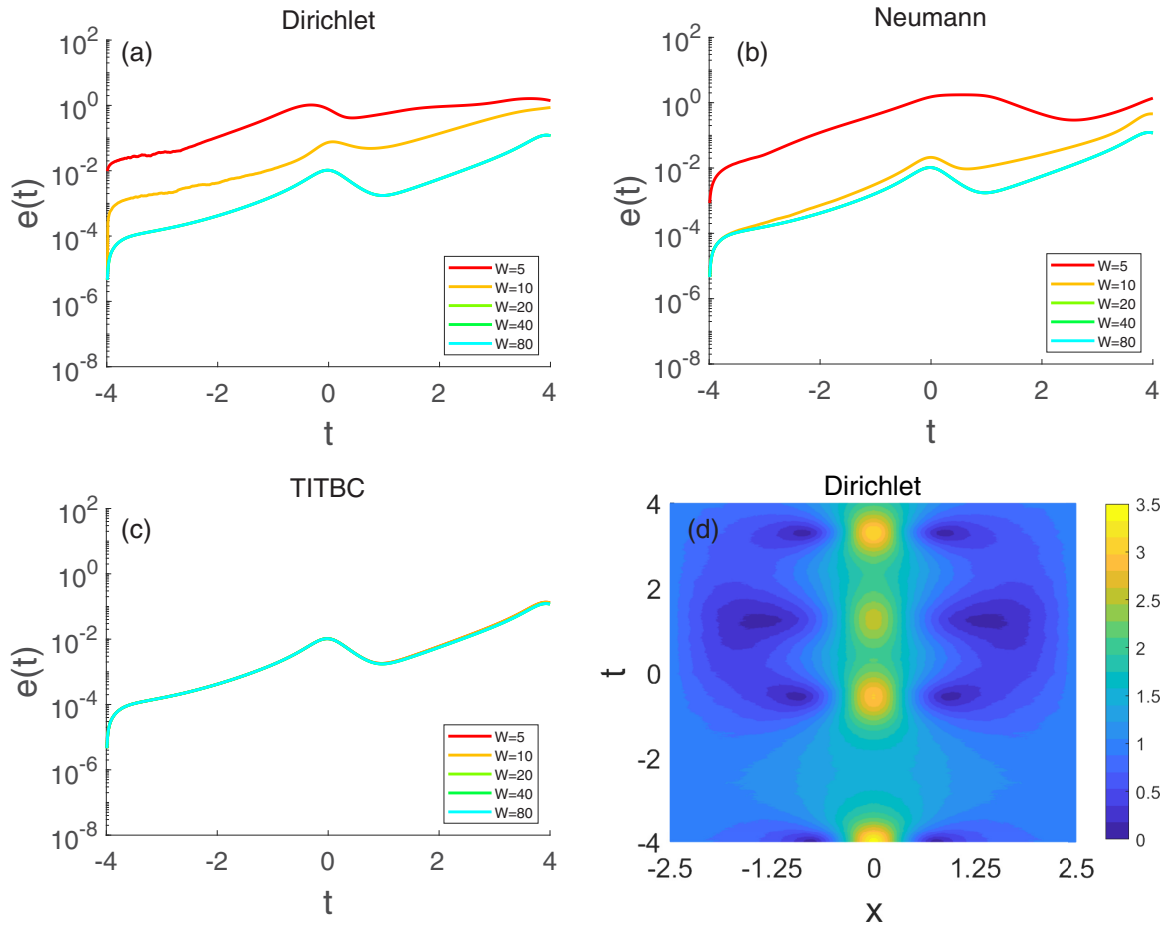


FIG. 3. The relative errors in $[-2.5, 2.5]$ with different width: (a) Dirichlet; (b) Neumann; and (c) TITBC. (d) The numerical result with $W = 5$ and the Dirichlet boundary condition.

the second-order accuracy in space of the Crank-Nicolson scheme (8).

Table I shows the CPU time in the simulations of the KB solution. Since the TITBC is more complex than other boundary conditions, it costs more time than others with the same width. Nevertheless, to obtain the “acceptable accuracy,” the TITBC costs 304 s with the width $W = 5$, whereas the other boundary conditions cost about 240 s with the width

$W = 20$. In the simulations of the KB solution, the TITBC reduces the memory requirement at the cost of a little longer computing time to obtain the same accuracy.

B. Numerical simulations of the PS solution

In this subsection, we verify the validity of the TITBC for the PS solution. Figure 6 shows the simulations performed

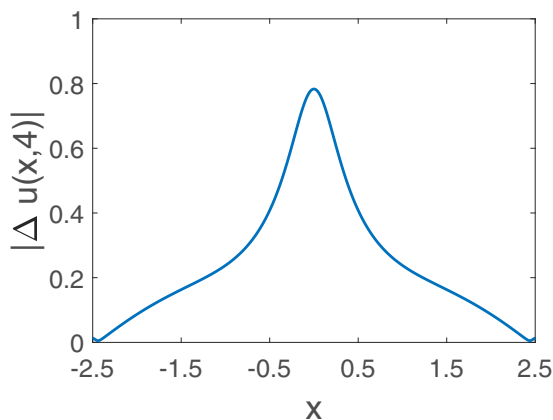


FIG. 4. The error at $t = 4$.

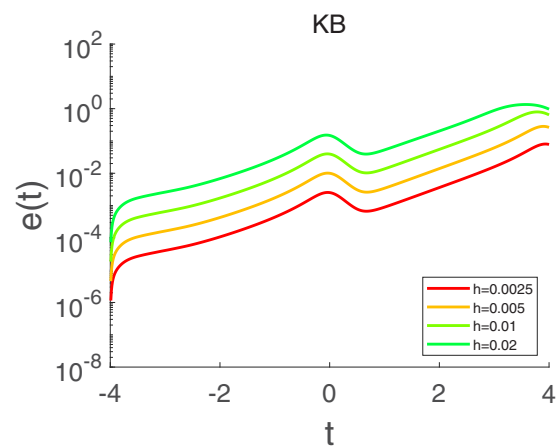


FIG. 5. The relative errors with different mesh sizes.

TABLE I. The CPU time in the simulations of the KB solution.

Boundary	W				
	5	10	20	40	80
Dirichlet	97 s	122 s	241 s	427 s	900 s
Neumann	73 s	124 s	243 s	507 s	1065 s
TITBC	304 s	632 s	1499 s	3303 s	6096 s

TABLE II. The CPU time in the simulations of the PS solution.

Boundary	W					
	5	10	20	40	80	160
Dirichlet	111 s	162 s	277 s	484 s	926 s	1960 s
Neumann	85 s	148 s	267 s	504 s	1118 s	2172 s
TITBC	330 s	626 s	1390 s	2841 s	5659 s	11568 s

in $[-10, 10] \times [-4, 4]$. Compared to Fig. 2, the simulations are more sensitive to the boundary conditions. In Figs.6(a) and 6(b), the spurious oscillations soon appear at the boundary and spread inwards. These spoil simulations of the PS solution in the central domain. In contrast, the simulation with the TITBC keeps the correct shape in Fig. 6(c).

Figure 7 shows the relative error evolution in the space domain $[-2.5, 2.5]$. Due to the limitation of our computer memory, we confine ourselves to a computational domain no wider than 160. The error increases when the computational spatial domain is smaller, which is the same as the KB result. Different from the KB simulations, Fig. 7(a) shows that there is a jump of the error soon after the start in the Dirichlet case. The cause of this jump is still unclear. Fortunately, it appears later and at a smaller magnitude when we enlarge the computational domain. The lower bound of errors with the Neumann boundary conditions is attained when the width

$W = 160$, as shown in Fig. 7(b). Figure 7(c) shows the errors with the TITBC. The error of the width $W = 5$ is slightly bigger than others. The errors decay to the lower bound when the width is no smaller than 10, which is 16 times smaller than the width for a comparable simulation with the Neumann boundary condition. For the PS solution, the TITBC has a great improvement compared to those commonly used boundary conditions.

Table II shows the CPU time in the simulations of the PS solution. The TITBC costs 626 s with the width $W = 10$ to obtain the “acceptable accuracy.” Limited to simulations in a spatial domain no wider than 160, we give a lower bound of 1960 s to attain the same accuracy for simulations with the Dirichlet boundary condition, which is already three times that of the TITBC. The Neumann boundary condition $W = 160$ costs 2172 s to achieve the same accuracy, which is also three times longer than what the TITBC costs. In the

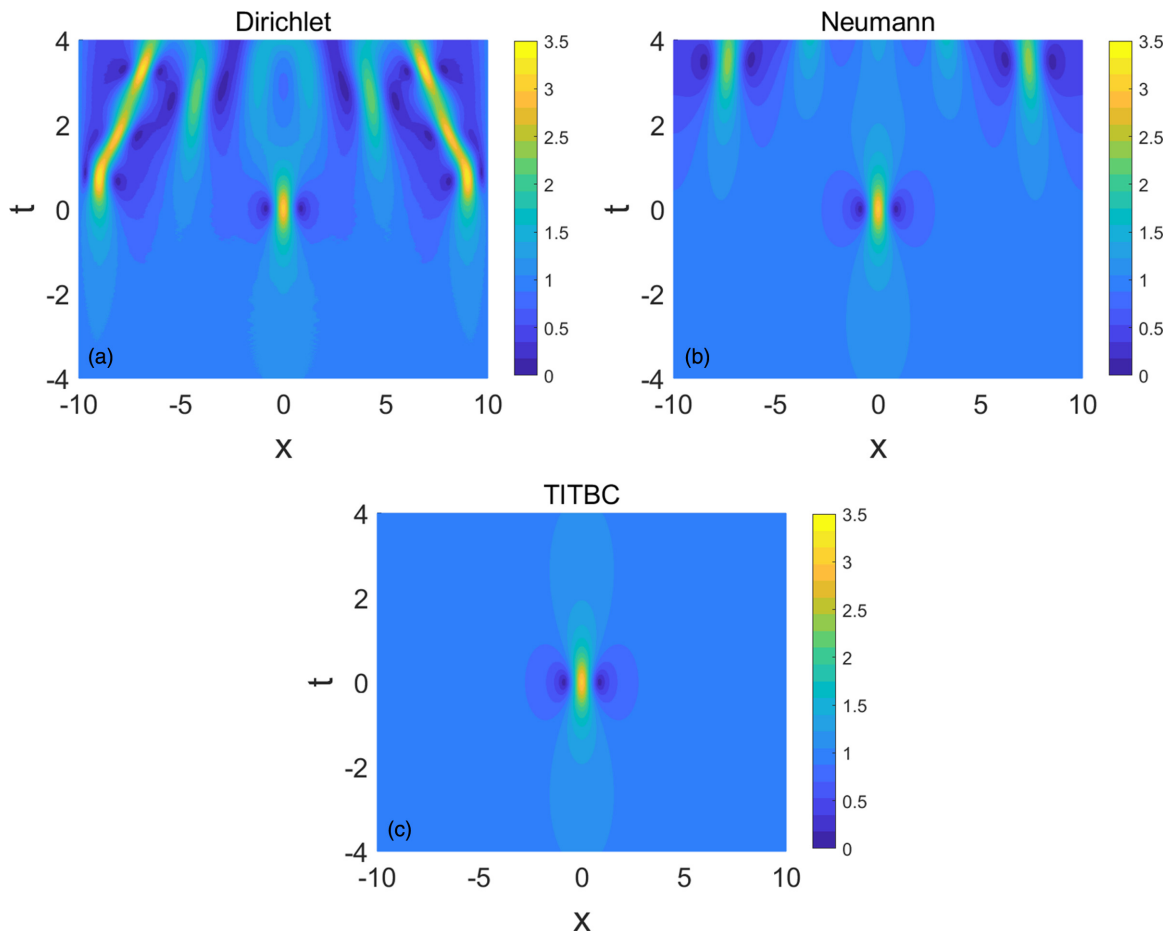


FIG. 6. The numerical result $|u|$ of the PS solution with different numerical boundary conditions: (a) Dirichlet; (b) Neumann; (c) TITBC.

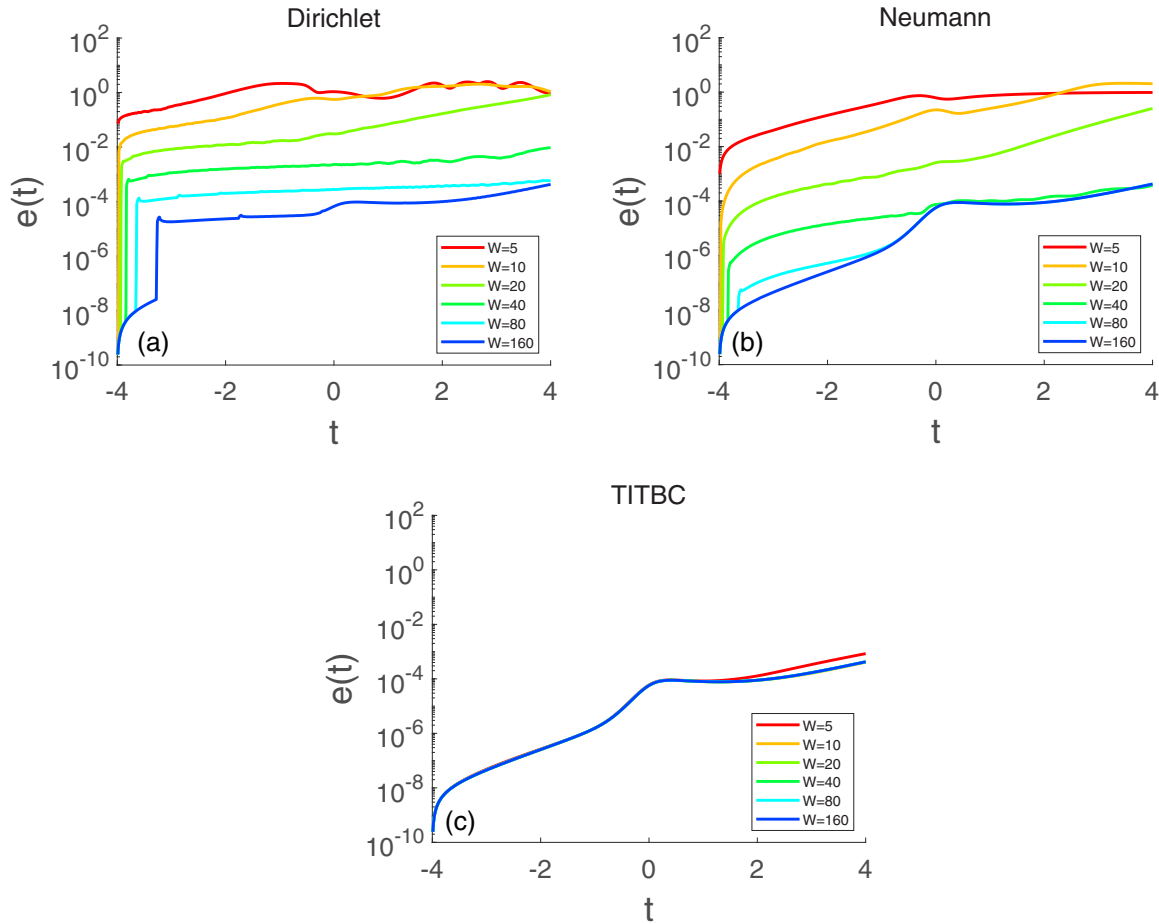


FIG. 7. The relative errors in $[-2.5, 2.5]$ with different width: (a) Dirichlet; (b) Neumann; (c) TITBC.

simulations of the PS solution, both the memory requirement and the computing time are reduced obviously by the TITBC.

IV. CONCLUSION

In summary, we propose a transparent boundary condition, namely the TITBC, for simulations of the PS and KB solutions. The lower bound of errors is determined by the spatial mesh size in simulations. To attain such “acceptable accuracy,” the Dirichlet, Neumann, and periodic boundary conditions require a big enough width for the computational domain. In comparison, simulations with the TITBC can be performed in a much smaller domain, especially only 1/16 for the PS solution simulation. The TITBC reduces both the

memory requirement and the computing time in the simulations of the PS solution.

We remark that there are abundant time-independent equations that breather solutions satisfy, such as breathers in the Sasa-Satsuma equation, the modified KdV equation, and the sine-Gordon equation. Deriving a transparent boundary condition for them needs further study.

ACKNOWLEDGMENTS

This work is supported in part by the National Natural Science Foundation of China under Grants No. 11832001, No. 11988102, and No. 11890681. We are grateful for stimulating discussions with the anonymous referees.

[1] B. Kibler, J. Fatome, C. Finot, G. Millot, F. Dias, G. Genty, N. Akhmediev, and J. M. Dudley, The Peregrine soliton in nonlinear fibre optics, *Nat. Phys.* **6**, 790 (2010).
 [2] N. Akhmediev, J. M. Dudley, D. R. Solli, and S. Turitsyn, Recent progress in investigating optical rogue waves, *J. Opt.* **15**, 060201 (2013).
 [3] N. Akhmediev, B. Kibler, F. Baronio, M. Belić, W. P. Zhong, Y. Q. Zhang, W. Chang, J. M. Soto-Crespo, P. Vouzas, P. Grelu *et al.*, Roadmap on optical rogue waves and extreme events, *J. Opt.* **18**, 063001 (2016).
 [4] C. Kharif and E. Pelinovsky, Physical mechanisms of the rogue wave phenomenon, *Eur. J. Mech. B Fluids* **22**, 603 (2003).
 [5] D. Peregrine, Water waves, nonlinear Schrödinger equations and their solutions, *ANZIAM J.* **25**, 16 (1983).
 [6] N. Akhmediev, A. Ankiewicz, and M. Taki, Waves that appear from nowhere and disappear without a trace, *Phys. Lett. A* **373**, 675 (2009).
 [7] E. A. Kuznetsov, Solitons in a parametrically unstable plasma, *Akad. Nauk SSSR Dokl.* **236**, 575 (1977).

- [8] Y. C. Ma, The perturbed plane-wave solutions of the cubic Schrödinger equation, *Stud. Appl. Math.* **60**, 43 (1979).
- [9] J. P. Berenger, A perfectly matched layer for the absorption of electromagnetic waves, *J. Comput. Phys.* **114**, 185 (1994).
- [10] C. Zheng, A perfectly matched layer approach to the nonlinear Schrödinger wave equations, *J. Comput. Phys.* **227**, 537 (2007).
- [11] B. Engquist and L. Halpern, Far field boundary conditions for computation over long time, *Appl. Numer. Math.* **4**, 21 (1988).
- [12] B. Engquist and A. Majda, Absorbing boundary conditions for the numerical simulation of waves, *Math. Comput.* **31**, 629 (1977).
- [13] M. Ehrhardt, Absorbing boundary conditions for hyperbolic systems, *Numer. Math. Theor. Meth. Appl.* **3**, 295 (2010).
- [14] X. Antoine, C. Besse, and S. Descombes, Artificial boundary conditions for one-dimensional cubic nonlinear Schrödinger equations, *SIAM J. Numer. Anal.* **43**, 2272 (2006).
- [15] C. Zheng, Exact nonreflecting boundary conditions for one-dimensional cubic nonlinear Schrödinger equations, *J. Comput. Phys.* **215**, 552 (2006).
- [16] X. Antoine, A. Arnold, C. Besse, M. Ehrhardt, and A. Schädle, A review of transparent and artificial boundary conditions techniques for linear and nonlinear Schrödinger equations, *Commun. Comput. Phys.* **4**, 729 (2008).
- [17] X. Antoine, W. Bao, and C. Besse, Computational methods for the dynamics of the nonlinear Schrödinger/Gross-Pitaevskii equations, *Comput. Phys. Commun.* **184**, 2621 (2013).
- [18] X. Wang and S. Tang, Matching boundary conditions for diatomic chains, *Comput. Mech.* **46**, 813 (2010).
- [19] G. Pang, L. Bian, and S. Tang, Almost exact boundary condition for one-dimensional Schrödinger equations, *Phys. Rev. E* **86**, 066709 (2012).
- [20] G. Pang and S. Tang, Approximate linear relations for Bessel functions, *Commun. Math. Sci.* **15**, 1967 (2017).
- [21] M. Birem and C. Klein, Multidomain spectral method for Schrödinger equations, *Adv. Comput. Math.* **42**, 395 (2016).
- [22] A. Islas and C. M. Schober, Numerical investigation of the stability of the rational solutions of the nonlinear Schrödinger equation, *Appl. Math. Comput.* **305**, 17 (2017).
- [23] P. Wang, Z. Xu, and J. Yin, Simple high-order boundary conditions for computing rogue waves in the nonlinear Schrödinger equation, *Comput. Phys. Commun.* **251**, 107109 (2020).
- [24] M. Delfour, M. Fortin, and G. Payr, Finite-difference solutions of a non-linear Schrödinger equation, *J. Comput. Phys.* **44**, 277 (1981).
- [25] T. R. Taha and M. I. Ablowitz, Analytical and numerical aspects of certain nonlinear evolution equations. ii. numerical, nonlinear Schrödinger equation, *J. Comput. Phys.* **55**, 203 (1984).
- [26] M. A. Alejo, L. Fanelli, and C. Muñoz, Stability and instability of breathers in the U(1) Sasa–Satsuma and nonlinear Schrödinger models, *Nonlinearity* **34**, 3429 (2021).
- [27] B. Gustafsson, The convergence rate for difference approximations to mixed initial boundary value problems, *Math. Comput.* **29**, 396 (1975).
- [28] C. Zheng and S. Tang, Long-time simulations of rogue wave solutions in the nonlinear Schrödinger equation, *Methods Appl. Anal.* **29**, 149 (2022).